Science and Technology Indonesia
e-ISSN:2580-4391 *p*-ISSN:2580-4405
Vol. 9, No. 2, April 2024

Research Paper

Identification of CO_2, SO_2, and a Mixture of Both Gases Using Optical Imaging Combined with Convolutional Neural Network (CNN)

Umi Salamah[1,2]*, Setyawan Purnomo Sakti[2], Agus Naba[2], Hariyadi Soetedjo[1]

[1]*Department of Physics, Faculty of Applied Science and Technology, Ahmad Dahlan University, Yogyakarta, 55166, Indonesia*
[2]*Department of Physics, Faculty of Mathematics and Natural Sciences, Brawijaya University, Malang, 65145, Indonesia*
***Corresponding author**: umi.salamah@fisika.uad.ac.id

Abstract
CO_2 and SO_2 gases are utilized in various industrial applications and are subjects of environmental research. However, these gases are considered toxic and pose dangers at certain concentrations. Therefore, it is crucial to monitor and control the exposure to these gases in the environment to prevent reaching hazardous levels that could endanger both humans and the environment. A non-contact detection and monitoring system is essential to minimize the adverse effects of direct gas exposure. In this research, a non-contact detection system for CO_2, SO_2, and mixed gases was developed using optical imaging analysis generated by infrared cameras. The images were captured using the FLIR Vue Pro-R infrared camera, with infrared-absorbing gas sourced from a 50-watt tungsten lamp. Visual identification of these gases through optical imaging is challenging; however, this study successfully identified these gases using a Convolutional Neural Network (CNN). The CNN architecture used in this study is DenseNet (Densely Connected Convolutional Networks), comprising 169 convolution layers. The CNN model was trained and tested on experimental optical imaging data, categorized into three classes: CO_2, SO_2, and a mixture of gases. A total of 1030 optical imaging data points were utilized for training. Training was conducted using the AdamW optimization function over 28 epochs. The evaluation of results yielded accuracy, precision, recall, and F1-score metrics. The novelty of this study lies in the successful identification of CO_2, SO_2, and their mixture by the CNN model with an accuracy of 85%. Precision, recall, and F1-score values are all 0.85. These results indicate that the CNN model effectively distinguishes optical imaging of each gas (CO_2, SO_2, and their mixture) consistently and accurately. Consequently, it can be concluded that the CNN model performs well in distinguishing between these gases in optical imaging analysis.

Keywords
CNN, CO_2, SO_2, Optical Imaging, Infrared Camera

Received: 30 November 2023, Accepted: 26 February 2024
https://doi.org/10.26554/sti.2024.9.2.371-379

1. INTRODUCTION

The use of non-volatile CO_2 as the focal point of investigations is widespread across various scientific fields, including health, mining, and the environment. This gas is emitted by volcanoes, with the presence often signaling an imminent eruption (Jeffery et al., 2013; Notsu et al., 2006; Jousset et al., 2012). This phenomenon was observed across case studies of volcanos in Mount Merapi in Yogyakarta and Mount Kelud in East Java, Indonesia. In this context, monitoring of CO_2 levels is very important to determine or predict the timing of volcanic eruptions. This knowledge is crucial given that areas surrounding volcanoes such as Merapi and Kelud are inhabited, posing a threat to the people and environment. Additionally, the knowledge is instrumental in introducing timely warnings to minimize disaster-related casualties.

The current monitoring methods used for volcano activities include seismic and deformation analyses. However, monitoring of CO_2 emissions has proven to be a valuable addition to predicting eruptions (Cronin et al., 2013; Di Traglia et al., 2018; Humaida, 2005; Jousset et al., 2012). One challenge faced in on-site (in-situ) monitoring within volcanoes is the hazardous nature of toxic gases, indicating the need for non-contact methods. Several previous studies have indicated the potential for non-contact gas detection, with one of the methods involving optical imaging. Non-contact method serves as a solution for the non-contact method required for toxic gases such as CO_2. However, gas in nature, especially in volcanoes, does not come out as a single gas, where the gas released from the volcano is a mixture of several gases. Therefore, the identification of these gases is a challenge in the development of non-contact gas detection. In addition, instruments are needed that are able to capture gas properties into an image

data. Vollmer and Möllmann (2011) stated that infrared cameras can monitor radiation, which enables the acquisition of CO_2 spectrum images (Battalwar et al., 2015; Vollmer and Möllmann, 2011). The inherently dynamic nature of gases poses a significant challenge in the analysis of optical imaging captured by infrared cameras. Consequently, there is a pressing need for tools to aid in gas detection. One particularly effective method for image data analysis, encompassing tasks such as classification, segmentation, and object detection, is the Convolutional Neural Network (CNN).

The use of CNN in gas detection systems has seen significant development, particularly with input data obtained from electronic noses. However, the application of CNN in gas identification based on optical imaging data remains limited. For instance, a study conducted by Peng et al. (2018) compared the accuracy of CNN, SVM, and MLP in gas detection using input data generated by an electronic nose. The findings of this research indicated that CNN achieved the highest accuracy. Another study with similar input data was reported by Xiong et al. (2023), where various gases such as H_2S, SO_2, and NH_3 were detected based on the characteristic odor components, rather than optical imaging. Research on the use of CNN for optical imaging detection was presented by Zhu et al. (2023), where CNN was implemented to detect the concentration of CS_2 and SO_2 using data from differential gas absorption spectrum (MDAS) to address spectrum inconsistency issues. The study successfully detected CS_2 and SO_2 gases with mean absolute errors of 0.51 and 1.12, respectively, although the spectrum data used was one-dimensional.

In this research, gas identification was conducted using two-dimensional image data as input. This represents a novelty compared to previous research. Identification based on two-dimensional data provides more detailed information by considering wavelength and light intensity. This allows for more accurate identification and deeper analysis of complex samples such as gases. In preceding research, the examination of CO_2 and mixed gases through optical imaging, employing grayscale image mode and histogram analysis, was conducted (Salamah et al., 2022; Salamah et al., 2023). The outcomes revealed distinctive histogram patterns generated by each gas. However, the study faced limitations in identifying the specific gas type, as the resulting optical images exhibited nearly identical color distribution in the R-G-B mode, making visual differentiation challenging. To address this limitation, the present study introduces a novel approach for identifying CO_2, SO_2, and gas mixtures using Convolutional Neural Network (CNN). The qualitative data derived from the investigation were further utilized for gas classification through CNN, a state-of-the-art image processing method (Chu et al., 2021; Frei and Kruis, 2021; Malamousi et al., 2022; Nie et al., 2022; Wei et al., 2019). Meanwhile, the dataset employed in this study is unique, consisting of experimental results that contribute novelty to the research.

2. EXPERIMENTAL SECTION

2.1 Materials

In this study, an investigation was conducted employing a vacuum chamber to introduce CO_2 gas (99.7%), SO_2 and a mixture of both gases. The gas source is genuine gas, often utilized in industries, stored in a cylinder equipped with a regulator and a flow meter, as demonstrated in Figure 1a. The gas flow, set at a rate of 5 L/min, was directed into the chamber for varying durations, and the characteristics were examined through infrared (IR) imaging captured by the FLIR camera. To establish references, individual tests were conducted for pure CO_2 and SO_2 before combining the gases. The experimental configuration for detecting CO_2 gas using a thermal imaging camera with R-G-B mode employed a vacuum tube. Throughout the experiment, the camera was positioned directly to the right of the gas-filled chamber. The experimental setup is illustrated in Figure 1b.

When CO_2 gas interacts with infrared radiation, it exhibits the ability to absorb such radiation. The energy from infrared radiation induces molecular vibrations, particularly in CO_2 gas, through its four vibrational modes, with three of them being responsive to infrared radiation energy (specifically, asymmetric stretching vibrations and two bending vibrations). The distinctive and specific nature of the infrared absorption band allows for the identification of compounds, as each type of chemical bond or functional group possesses a unique signature. In the infrared (IR) spectrum, CO_2 gas demonstrates peak absorption at wavelengths ranging from 2.5 to 2.6 μm, 4.3 to 4.5 μm, as well as at 9.5 μm, 10.5 μm, and 14 μm, respectively, with additional weak absorption peaks, as illustrated in Figure 2. To achieve non-contact gas detection of CO_2, a thermal imaging camera covering the spectrum from 8 to 14 μm was employed, given its relatively lower cost in the market. This distinct peak absorption characteristic provides an advantageous means of differentiating CO_2 gas from other gases present in the atmosphere

2.2 Methods

As shown in Figure 1, data were collected from three types of optical imaging clusters of gases namely CO_2, SO_2, and a mixture of both. The number of optical imaging data of each cluster was 330 to 350, respectively, totaling 1030. The data were used for training and tests which were further analyzed. Gas that absorbs certain wavelengths is captured with an infrared camera that produces optical imaging, where the optical imaging will be analyzed and processed using CNN. CNN model architecture used in this study was DenseNet, implemented through Google Colab. This model comprised 169 layers, incorporating typical processes such as convolution, relu, batch norm, and residual block by adding filters from the previous layer and combining for the next process. By using this method, the last layer was used for the linear combination. This layer resulted from the extraction of CNN DenseNet features. These features were instrumental in predicting the number of classes, with each having a distinct probability out-

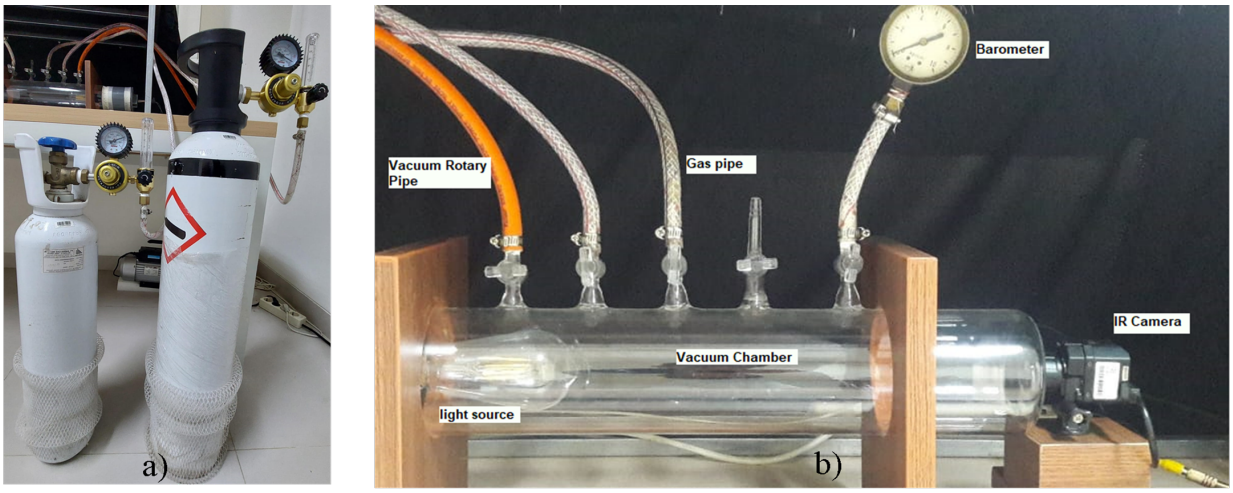

Figure 1. a) The Source of Gases and b) The Apparatus Set Up for the Experiment of Gas Detection

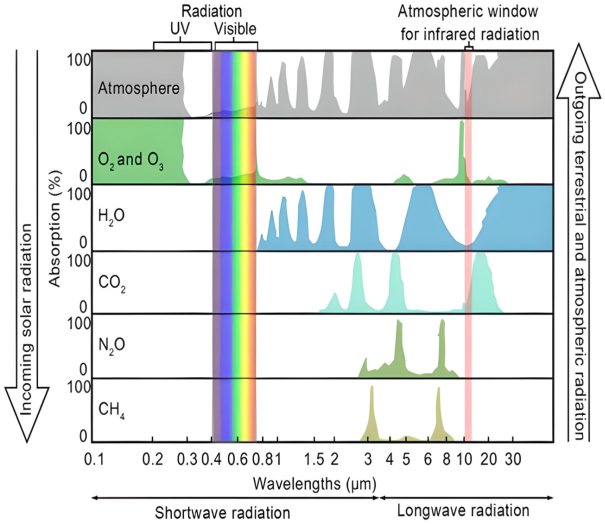

Figure 2. The Percentage of Radiation Absorption by Gases in the Atmosphere (Takle, 2015)

put. Each class with the highest probability was taken as the prediction. The DenseNet architecture used in this study is shown in Figure 3.

CNN DenseNet is a pre-trained model initially trained on the extensive imageNet dataset (Alzubaidi et al., 2022; He et al., 2022; Paul and Sabeenian, 2022; Wu et al., 2023). Subsequently, the learned weights/parameters were stored and further used for fine-tuning specific tasks using the DenseNet architecture only. For data augmentation in images, several pre-processing methods were carried out including random rotation (15 degrees), random resize crop with crop size of 224×224 pixels, random horizontal flip, random vertical flip, brightness (0.7), scale image $(0 - 1)$ and standardization image scale $((-3) - 3)$. Meanwhile, for testing data, the methods included Rresize crop (224×224 pixels), scale image $(0 - 1)$ and standardization image scale $((-3) - 3)$. The hyperparameters used in the CNN DenseNet training process are shown in Table 1.

Table 1. Hyperparameters of CNN DenseNet

Hyperparameter	Values
Number of classes	3
Batch_size	32
Crop_size	224×224
Learning_rate	0.0001
Dropout	0.2
Decay	0.01
Optimizer	AdamW $\beta 1 = 0.9$, $\beta 2 = 0.999$
Epoch	Infinite
Early Stopping	5
Max Grad Norm	0.8

Analysis and evaluation of gas identification using CNN using a fusion matrix. Basically the matrix has four cells: True Positive (TP): Correctly predicted positive cases, True Negative (TN): Correctly predicted negative cases, False Positive (FP): False Negative cases incorrectly predicted as positive, False Negative (FN): False positive cases predicted as negative. An example of a 3×3 fusion matrix is shown in Figure 4.

There are several parameters used for the analysis of the results of classification based on the fusion matrix, including accuracy, recall, precision and F1 Score (Yacouby and Axman, 2020).

a. Accuracy is an evaluation used to determine how often the CNN model performs the correct classification (TP) of all data, mathematically accuracy is formulated Equation 1.

$$\text{Accuracy} = \frac{\text{TP}}{\text{Total number of data}} \quad (1)$$

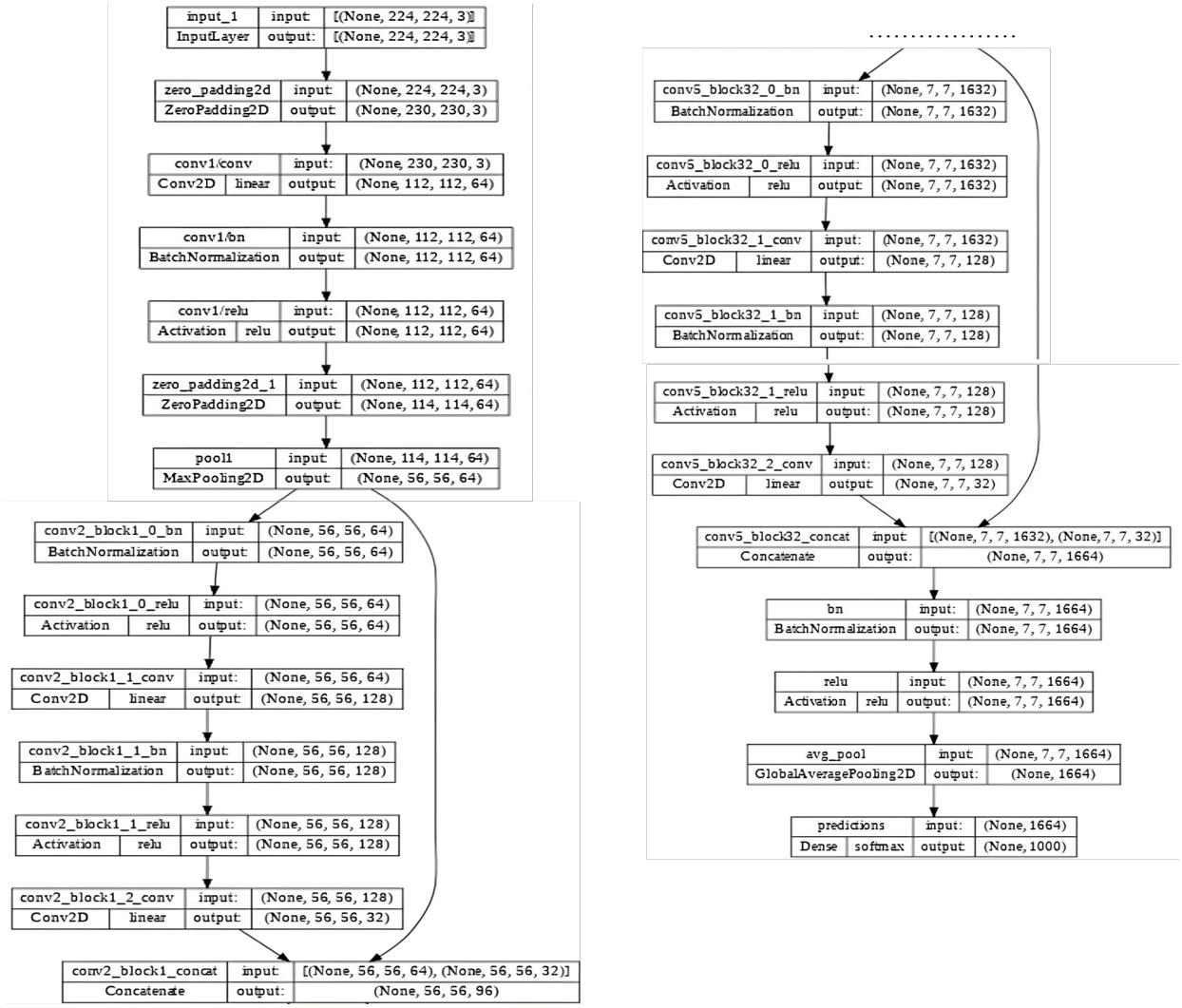

Figure 3. DenseNet Model Architecture for Gas Detection System with 169 Layers

	Prediction A	Prediction B	Prediction C
Actual A	**TP**	**FN**	**FN**
Actual B	**FP**	**TP**	**FN**
Actual C	**FP**	**FP**	**TP**

Figure 4. Example of a 3 × 3 Fusion Matrix

b. Recall, also known as sensitivity, is an evaluation metric that measures how well a classification model is able to identify all actual positive cases in a dataset. To calculate recall is formulated as in Equation 2.

$$\text{Recall} = \frac{\text{TP}}{\text{TP} + \text{FN}} \tag{2}$$

c. Precision, an evaluation that measures how much of a class is predicted as positive by a truly positive model. In the context of classification, precision describes how precise the model is in identifying positive cases out of all cases that have been predicted as positive. Mathematically, precision is calculated by dividing the number of True Positives (TP) by the total number of correct positive predictions (TP + False Positive (FP)), as in Equation 3.

$$\text{Precission} = \frac{\text{TP}}{\text{TP} + \text{FP}} \tag{3}$$

d. The F1 Score is an evaluation that combines precision and recall, which reflects the balance between precision and recall, and is useful for evaluating model performance in imbalanced classes or when avoiding imbalances between the number of correct positive predictions (TP) and the number of correct negative predictions (TN). Mathematically, the F1 score is calculated as the

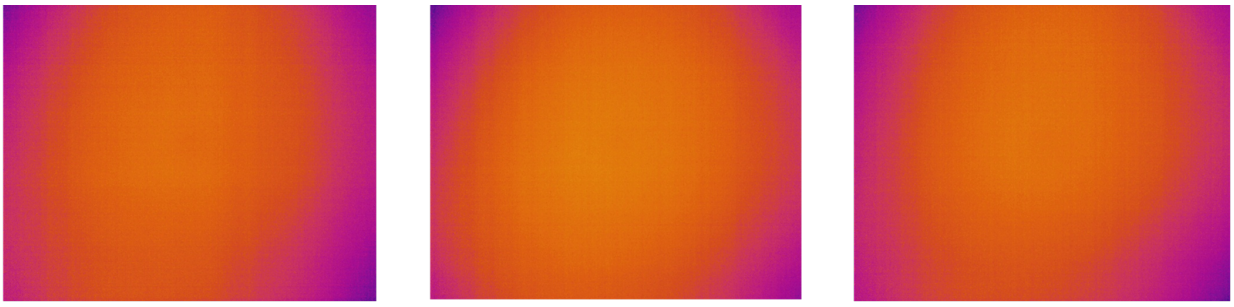

Figure 5. Sample of Optical Imaging for a) CO_2, b) SO_2 and c) CO_2 and SO_2 Mixture

harmonic mean of precision and recall as in Equation 4.

$$\text{FP Score} = 2 \times \frac{\text{Recall} \times \text{Precission}}{\text{Recall} + \text{Precission}} \quad (4)$$

3. RESULTS AND DISCUSSION

3.1 Data for Optical Imaging Gas Detection

Data collection was carried out through the IR camera used in the form of optical images. The IR source used was a Tungsten lamp (4 W), while CO_2, SO_2, and a mixture of both gases were placed in a special chamber for sample experiments. The test gases flowed in a Pyrex vacuum chamber conditioned at 20 mbar (15 Torr or equivalent to 0.02 atm) (Xiao et al., 2008). Figure 5 shows an example of optical imaging produced with three types of gases, namely CO_2, SO_2, and a mixture of both.

In terms of visualization, the optical imaging look similar, but they are not. The optical imaging produced is extremely challenging to differentiate based solely on the color distribution generated. Therefore, the optical imaging produced is processed using Convolutional Neural Networks (CNN) to identify the gas. CNN's method could distinguish the similar images into different pattern leads to the specific characteristic of gas.

3.2 CNN Optical Imaging Training Results

CNN data were further trained using the AdamW Adaptive Momentum with the Decay optimization function. This choice was predicated on the fact that AdamW was considered more effective for determining classification compared to standard Adam optimization (Parmar et al., 2020). For this method, Hyperparameter optimization was set for $\beta 1 = 0.9$ and $\beta 2 = 0.999$ with a learning rate of 0.001. Visualization of the cost value (loss value) and score value (accuracy value) is shown in the graphs of Figures 6a and 6b. Meanwhile, details on the cost/loss and score/accuracy results in training and testing data are given in Table 2.

Based on the above image, it can be observed that iterations yield accuracy (score) and loss (cost) values for both training and testing data. On the horizontal axis is the value representing the number of iterations (epochs), while on the vertical axis is the value representing either cost or score. Accuracy is a metric used to assess the success rate of the model created. On the other hand, the value is a measure of the error incurred by the network, with the aim of minimizing it. Figure 6 shows the movement of accuracy value (score) and loss value (cost) for trained data and test data produced by each iteration (epoch). Based on Figure 6a, the red line represents the movement for the training data, while the blue line depicts the movement for the testing data. The top graph illustrates the loss/cost values for both datasets. It can be observed that the loss values for the training data continuously decrease until the 28^{th} epoch, whereas the loss values for the testing data initially decrease, but then start to rise at a certain point until the 28^{th} epoch. In Figure 6b, the graph illustrates the accuracy values of both the training and testing datasets. The image indicates that the iteration results yield a steady increase in accuracy for the training data until the 28^{th} epoch, while the accuracy for the testing data fluctuates until the 28^{th} epoch. At the conclusion of the iterations, the training data achieves an accuracy of 0.8100, whereas the testing data achieves an accuracy of 0.8476 in the final epoch.

Based on the result, CNN DenseNet training spanned 28 epochs. At the 23^{rd} epoch (early stopping = 5), the best accuracy value was obtained, namely 0.8100 in training and 0.8476 in testing data. The visualization of the cost value is depicted in Figure 5a, while Figure 5b illustrates the accuracy trends. The training process using CNN DenseNet model required an extended time which stopped at 28^{th} epochs. This extended time resulted in fluctuating turbulent cost and accuracy curves (up and down significantly).

3.3 Detection Results of CO_2, SO_2, and a Mixture of Both Gases

To facilitate further processing of optical imaging, a CNN architecture was utilized. In this research, experiments were conducted on optical imaging of gases categorized into three types: CO_2, SO_2, and a mixture of both. This architecture was designed to recognize specific gas patterns (Fiorentino et al., 2023; Zeng et al., 2023) including CO_2, SO_2, and a mixture of both. In this context, data were collected for 350 (CO_2 gas), 330 (SO_2 gas), and 350 optical images (CO_2 and SO_2 mixed

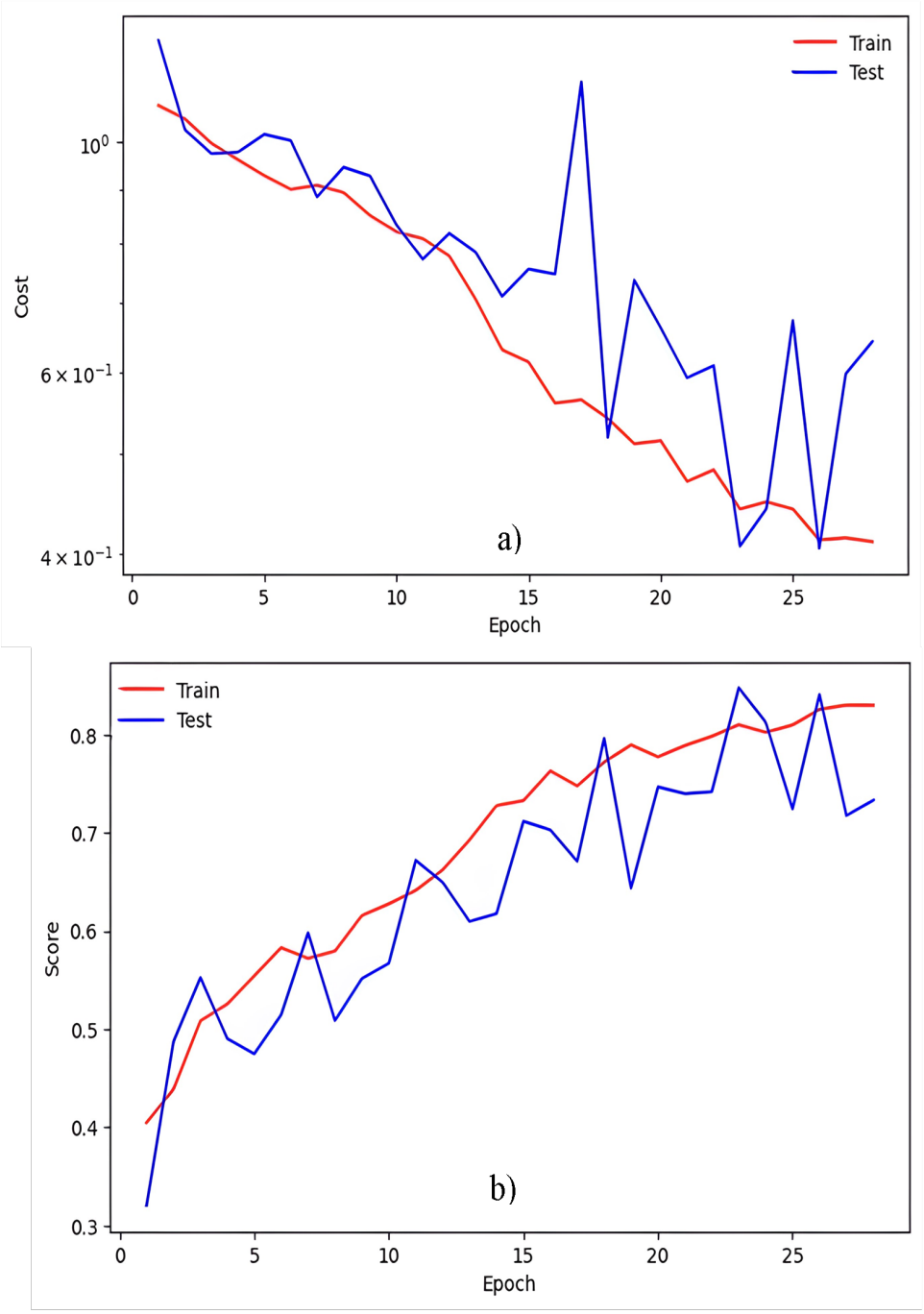

Figure 6. The results of CNN Denset Process for (a) Process Cost Visualization Graph and (b) Score/Accuracy

gases) to produce a total of 1030 imaging data. The results were obtained for gas testing through the confusion matrix as shown in Figure 7 and the classification in Figure 8.

The confusion matrix depicted in Figure 7 is a 3×3 matrix that indicates the involvement of 3 classifications in the identification process. Horizontally, there are the predictions made, while vertically, there are the actual data obtained from the experiment. The diagonal fields highlighted in green indicate True Positive (TP), which signifies the count of correct predictions within the true class. In the prediction of SO_2, out of a total of 330 data points, 298 were correctly identified as TP. Similarly, in the prediction of CO_2, out of a total of 350 data points, 308 were correctly identified as TP. While, in the prediction of mixed gases, out of a total of 350 data points, 267

Table 2. CNN DenseNet Training Results

Epoch	Train Cost	Test Cost	Train Score	Test Score
1	1,0860	1,2545	0.4049	0.3204
2	1,0540	1,0287	0.4389	0.4874
3	0.9986	0.9758	0.5084	0.5524
4	0.9628	0.9785	0.5256	0.4903
5	0.9291	1,0184	0.5543	0.4748
6	0.9012	1,0047	0.5830	0.5146
7	0.9093	0.8863	0.5721	0.5981
8	0.8949	0.9466	0.5795	0.5087
9	0.8503	0.9284	0.6157	0.5515
10	0.8201	0.8325	0.6276	0.5670
11	0.8076	0.7716	0.6413	0.6718
12	0.7771	0.8171	0.6622	0.6495
13	0.7055	0.7835	0.6928	0.6097
14	0.6306	0.7103	0.7277	0.6175
15	0.6137	0.7546	0.7327	0.7117
16	0.5602	0.7464	0.7629	0.7029
17	0.5641	1,1443	0.7477	0.6709
18	0.5414	0.5191	0.7720	0.7961
19	0.5117	0.7363	0.7895	0.6437
20	0.5151	0.6623	0.7773	0.7466
21	0.4706	0.5925	0.7888	0.7398
22	0.4828	0.6087	0.7982	0.7417
23	0.4425	0.4075	0.8100	0.8476
24	0.4497	0.4429	0.8022	0.8126
25	0.4426	0.6729	0.8097	0.7243
26	0.4131	0.4055	0.8256	0.8408
27	0.4150	0.5978	0.8300	0.7175
28	0.4116	0.6420	0.8297	0.7330

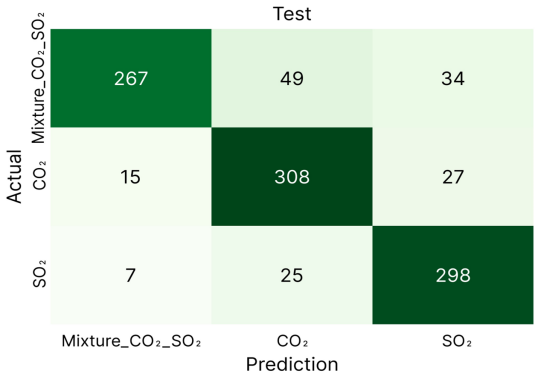

Figure 7. CNN Confusion Matrix on Gas Detection

	precision	recall	f1-score	support
0	0.92	0.76	0.84	350
1	0.81	0.88	0.84	350
2	0.83	0.90	0.87	330
accuracy			0.85	1030
macro avg	0.85	0.85	0.85	1030
weighted avg	0.85	0.85	0.85	1030

Figure 8. CNN DenseNet Classification Report on Gas Detection

were correctly identified as TP.

From Figure 8, the obtained values for accuracy, recall, precision, and F1-score are parameters used in model development. The evaluation results in this study yielded an accuracy of 0.85, an average precision of 0.85, recall of 0.85, and F1-score of 0.85. Accuracy depicts how often the model predicts classes correctly, whether positive or negative. With an accuracy value of 85%, and a total dataset of 1030 instances, it can be inferred that the designed CNN model succeeded in classification. In general, the accuracy of the gas detection system using CNN was considered good, surpassing the 80% threshold (Paul and Sabeenian, 2022; Tang et al., 2022; Da Wang et al., 2021; Yang et al., 2017). Precision, recall, and F1-score

values are other important indicators of model performance. Precision quantifies the ratio of correct positive predictions to the total number of positive predictions generated by the CNN. A high precision value indicates that the model has the ability to identify each type of gas without misclassifying each gas type. For example, if the precision value is high, actual optical imaging data of CO_2 will not be misidentified as SO_2 or a mixture of gases in the prediction data. Meanwhile, recall measures the proportion of true positive instances correctly identified by the model out of all positive instances in the data. For example, actual optical imaging data of CO_2 is identified as CO_2 in the predictions made. A high recall value indicates that the model can identify gases without missing the identification of each gas. F1-score, as a value that balances precision and recall, provides an overall picture of the model's performance in classification. The obtained parameter values affirm the success of gas identification using CNN, showcasing the model consistent and balanced ability to distinguish optical imaging of each gas (CO_2, SO_2, and a mixture of both).

4. CONCLUSIONS

Based on the results of experiments and optical imaging processing analysis conducted in the research, it was found that detecting CO_2, SO_2 and mixed gases with infrared cameras is very possible. This is evidenced by gas detection systems based on optical imaging have been successfully implemented using CNN classification system with a 169-layer DensesNet architecture. The designed CNN effectively classified CO_2, SO_2, and a mixture of both gases with a very good accuracy of 85%. This study has been able to identify each gas but has not been able to show the level of concentration. Therefore, further studies are needed in order to measure the level of gas concentration.

5. ACKNOWLEDGMENT

We would like to extend our gratitude to the Department of Physics at Universitas Brawijaya, Malang, for providing the opportunity to pursue our doctoral studies there. Additionally, we express our appreciation to the Advance Laboratory of Physics (AloP) at Universitas Ahmad Dahlan, Yogyakarta, which served as the research site for this study. The support and facilities provided by both institutions have been invaluable in advancing our research endeavors.

REFERENCES

Alzubaidi, F., P. Makuluni, S. R. Clark, J. E. Lie, P. Mostaghimi, and R. T. Armstrong (2022). Automatic Fracture Detection and Characterization from Unwrapped Drill-Core Images Using Mask R-CNN. *Journal of Petroleum Science and Engineering*, **208**; 109471

Battalwar, P., J. Gokhale, and U. Bansod (2015). Infrared Thermography and IR Camera. *International Journal of Research in Science & Engineering*, **1**(3); 9–14

Chu, J., W. Li, X. Yang, Y. Wu, D. Wang, A. Yang, H. Yuan, X. Wang, Y. Li, and M. Rong (2021). Identification of Gas Mixtures Via Sensor Array Combining with Neural Networks. *Sensors and Actuators B: Chemical*, **329**; 129090

Cronin, S. J., G. Lube, D. S. Dayudi, S. Sumarti, and S. Subrandiyo (2013). Insights into the October-November 2010 Gunung Merapi Eruption (central Java, Indonesia) from the Stratigraphy, Volume and Characteristics of Its Pyroclastic Deposits. *Journal of Volcanology and Geothermal Research*, **261**; 244–259

Da Wang, Y., M. J. Blunt, R. T. Armstrong, and P. Mostaghimi (2021). Deep Learning in Pore Scale Imaging and Modeling. *Earth-Science Reviews*, **215**; 103555

Di Traglia, F., T. Nolesini, L. Solari, A. Ciampalini, W. Frodella, D. Steri, B. Allotta, A. Rindi, L. Marini, and N. Monni (2018). Lava Delta Deformation As a Proxy for Submarine Slope Instability. *Earth and Planetary Science Letters*, **488**; 46–58

Fiorentino, M. C., F. P. Villani, M. Di Cosmo, E. Frontoni, and S. Moccia (2023). A Review on Deep-Learning Algorithms for Fetal Ultrasound-Image Analysis. *Medical Image Analysis*, **83**; 102629

Frei, M. and F. E. Kruis (2021). Fiber-Cnn: Expanding Mask R-CNN to Improve Image-Based Fiber Analysis. *Powder Technology*, **377**; 974–991

He, H., H. Xu, Y. Zhang, K. Gao, H. Li, L. Ma, and J. Li (2022). Mask R-CNN Based Automated Identification and Extraction of Oil Well Sites. *International Journal of Applied Earth Observation and Geoinformation*, **112**; 102875

Humaida, H. (2005). A Study on Carbon Isotope of CO_2 and CH_4 in Western Dieng Plateu by Gas Chromatography-Isotope Ratio Mass Spectrometer (GC-IRMS). *Indonesian Journal of Chemistry*, **5**(1); 11–14

Jeffery, A. J., R. Gertisser, V. R. Troll, E. M. Jolis, B. Dahren, C. Harris, A. G. Tindle, K. Preece, B. O'Driscoll, and H. Humaida (2013). The Pre-Eruptive Magma Plumbing System of the 2007-2008 Dome-Forming Eruption of Kelut Volcano, East Java, Indonesia. *Contributions to Mineralogy and Petrology*, **166**; 275–308

Jousset, P., J. Pallister, M. Boichu, M. F. Buongiorno, A. Budisantoso, F. Costa, S. Andreastuti, F. Prata, D. Schneider, and L. Clarisse (2012). The 2010 Explosive Eruption of Java's Merapi Volcano — A '100-Year'event. *Journal of Volcanology and Geothermal Research*, **241**; 121–135

Malamousi, K., K. Delibasis, B. Allcock, and S. Kamnis (2022). Digital Transformation of Thermal and Cold Spray Processes with Emphasis on Machine Learning. *Surface and Coatings Technology*, **433**; 128138

Nie, F., H. Wang, Q. Song, Y. Zhao, J. Shen, and M. Gong (2022). Image Identification for Two-Phase Flow Patterns Based on CNN Algorithms. *International Journal of Multiphase Flow*, **152**; 104067

Notsu, K., T. Mori, S. C. D. Vale, H. Kagi, and T. Ito (2006). Monitoring Quiescent Volcanoes by Diffuse CO_2 Degassing: Case Study of Mt. Fuji, Japan. *Pure and Applied Geophysics*,

163; 825–835

Parmar, V., N. Bhatia, S. Negi, and M. Suri (2020). Exploration of Optimized Semantic Segmentation Architectures for Edge-Deployment on Drones. http://arxiv.org/abs/2007.02839

Paul, E. and R. Sabeenian (2022). Modified Convolutional Neural Network with Pseudo-CNN for Removing Nonlinear Noise in Digital Images. *Displays*, **74**; 102258

Peng, P., X. Zhao, X. Pan, and W. Ye (2018). Gas Classification Using Deep Convolutional Neural Networks. *Sensors*, **18**(1); 157

Salamah, U., S. Sakti, H. Soetedjo, and A. Naba (2022). Non-Contact Technique for CO_2 Gas Monitoring Using Thermal Imaging Camera. In *Journal of Physics: Conference Series*, volume 2165. IOP Publishing, page 012019

Salamah, U., S. P. Sakti, H. Soetedjo, and A. Naba (2023). Optical Imaging Identification of CO_2 and SO_2 in Non-Contact Detection System Using Infrared Camera. In *AIP Conference Proceedings*, volume 2619. AIP Publishing, page 050014

Takle, E. (2015). *Agricultural Meteorology and Climatology*. Elsevier, pages 92–97

Tang, P., D. Zhang, and H. Li (2022). Predicting Permeability from 3D Rock Images Based on CNN with Physical Information. *Journal of Hydrology*, **606**; 127473

Vollmer, M. and K.-P. Möllmann (2011). 3.2-IR Imaging of CO_2: Basics, Experiments, and Potential Industrial Applications. *Proceedings IRS^2 2011*; 59–64

Wei, G., G. Li, J. Zhao, and A. He (2019). Development of a LeNet-5 Gas Identification CNN Structure for Electronic Noses. *Sensors*, **19**(1); 217

Wu, Y., R. Du, J. Feng, S. Qi, H. Pang, S. Xia, and W. Qian (2023). Deep CNN for COPD Identification by Multi-View Snapshot Integration of 3D Airway Tree and Lung Field. *Biomedical Signal Processing and Control*, **79**; 104162

Xiao, P., J. Zhang, P. Webley, G. Li, R. Singh, and R. Todd (2008). Capture of CO_2 from Flue Gas Streams with Zeolite 13X by Vacuum-Pressure Swing Adsorption. *Adsorption*, **14**; 575–582

Xiong, L., M. He, C. Hu, Y. Hou, S. Han, and X. Tang (2023). Image Presentation and Effective Classification of Odor Intensity Levels Using Multi-Channel Electronic Nose Technology Combined with Gasf and CNN. *Sensors and Actuators B: Chemical*, **395**; 134492

Yacouby, R. and D. Axman (2020). Probabilistic Extension of Precision, Recall, and F1 Score for More Thorough Evaluation of Classification Models. In *Proceedings of the First Workshop on Evaluation and Comparison of Nlp Systems*. pages 79–91

Yang, Z., H. Ji, Z. Huang, B. Wang, and H. Li (2017). Application of Convolution Neural Network to Flow Pattern Identification of Gas-Liquid Two-Phase Flow in Small-Size Pipe. In *2017 Chinese Automation Congress (CAC)*. IEEE, pages 1389–1393

Zeng, J., H. Wu, and M. He (2023). Image Classification Combined with Faster R-CNN for the Peak Detection of Complex Components and Their Metabolites in Untargeted LC-HRMS Data. *Analytica Chimica Acta*, **1238**; 340189

Zhu, R., J. Gao, M. Li, Q. Gao, X. Wu, and Y. Zhang (2023). A ppb-level Online Detection System for Gas Concentrations in CS_2/SO_2 Mixtures Based on UV-DOAS Combined with VMD-CNN-TL Model. *Sensors and Actuators B: Chemical*, **394**; 134440

